Poynting flux

MHD eqs

$$\frac{\partial \varrho}{\partial t} = -\nabla \cdot (\varrho \mathbf{v}) \tag{1}$$

$$\frac{\partial \varrho \mathbf{v}}{\partial t} = -\nabla \cdot (\varrho \mathbf{v}\mathbf{v}) + \frac{f_{v_A}}{4\pi} \nabla \cdot \left(\mathbf{B}\mathbf{B} - \frac{1}{2}\mathbf{I}\,B^2 \right)$$
$$- \nabla P + \varrho \mathbf{g} \tag{2}$$

$$\frac{\partial E_{\mathrm{HD}}}{\partial t} = -\nabla \cdot [\mathbf{v}(E_{\mathrm{HD}} + P)] + \varrho \mathbf{v} \cdot \mathbf{g} + \frac{\eta}{4\pi}(\nabla \times \mathbf{B})^2$$
$$+ \mathbf{v} \cdot \frac{f_{v_A}}{4\pi} \nabla \cdot \left(\mathbf{B}\mathbf{B} - \frac{1}{2}\mathbf{I}\,B^2 \right) + Q_{\mathrm{rad}} \tag{3}$$

$$\frac{\partial \mathbf{B}}{\partial t} = \nabla \times (\mathbf{v} \times \mathbf{B} - \eta \nabla \times \mathbf{B})\,. \tag{4}$$

Poynting flux

$$\vec{P} = \vec{E} \times \vec{B} = (-\vec{v} \times \vec{B} + \eta \nabla \times \vec{B}) \times \vec{B}$$

$$E_{mag} = \frac{B^2}{8\pi}, \qquad \vec{j} = \frac{1}{4\pi} \nabla \times \vec{B}$$

$$\frac{\partial E_{mag}}{\partial t} + \frac{1}{4\pi} \nabla \cdot \vec{P} = -\vec{j} \cdot \vec{E}$$

$$\vec{j} \cdot \vec{E} = \vec{v} \cdot \left(\vec{j} \times \vec{B} \right) + \frac{\eta}{4\pi} \left(\nabla \times \vec{B} \right)^2$$

Boundary conditions used here

horizontal: periodic
vertical:

- hydrodynamical variables:
  All three mass flux components are symmetric with respect to the boundary. We decompose the gas pressure into mean pressure and fluctuation. The mean pressure is extrapolated into the ghost cells such that its value at the boundary is fixed, while the pressure fluctuations are damped in the ghost cells.
- magnetic field:
  - bottom
    - O16bM: symmetric
    - Z16M: zero
  - top: potential field extrapolation

Comparison of the Poynting flux for the simulations O16bM (solid) and Z16M (dashed)
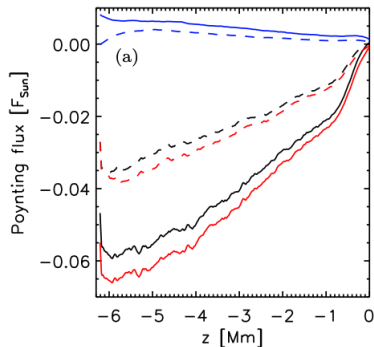

Figure 1: Black lines show the horizontally averaged Poynting flux, blue and red lines present the contributions from up- and downflows

- z component averaged in horizontal plane (horizontal component = 0 because of symmetry?), normalized by solar photospheric energy flux
- bottom domain, solid line: upflow - BC open makes flux enter the domain, but downflow flux = 6 * upflow flux
- dashed line: bottom upflow = 0(BC def) , but z > -5,-4 Mm upward directed (total?) Poynting flux, almost identical contribution (as solid line) for (both, not only upward?) flow

Comparison of energy loss rate: $-\frac{P(z)}{\int_z^{z_{top}} E_{mag} dz}$ for the simulations O16bM (solid) and Z16M (dashed)
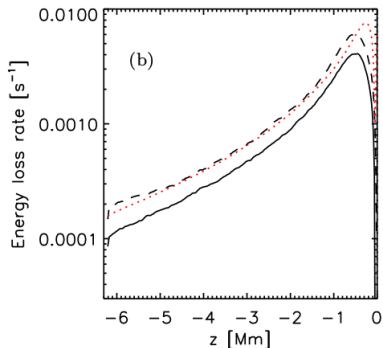

Figure 2: Energy loss rate due to the Poynting flux. The red dotted line indicates a convective overturning rate: $\frac{v_{z_{rms}}}{H_\rho}$

- integration in the domain above a height z
- flux close to 0 at the top boundary
- dashed line: magnetic loss rate 1.8 times higher (log scale) , profile agrees with the red line (smaller Pz, but much smaller magnetic energy: about 4 times)
- magnetic energy loss due to overturnig convection (red line) has a slow timescale: $\frac{H_\rho}{v_{z\,rms}}$
- dynamo growth rate $\gamma >> \frac{v_{z\,rms}}{H_\rho}$ (kinematic growth phase) achieved always with high resolution($\Delta x \leq 8km$), low resolution(16 km here) only in in the bottom part, not in the photosphere
- non linear saturation phase: $\gamma \approx \frac{v_{z\,rms}}{H_\rho}$ bottom BCs matter
- dashed line: maximum energy loss at the bottom boundary $\implies$ the lower limit(small saturation field strength) for an efficient dynamo (solid line below dashed: more efficient)

Comparison of the energy lost by the Poynting flux to the energy converted via the Lorentz force: $\frac{P(z)}{\int_z^{z_{top}} \vec{v} \cdot (\vec{j} \times \vec{B}) dz}$ for the simulations O16bM (solid) and Z16M (dashed)
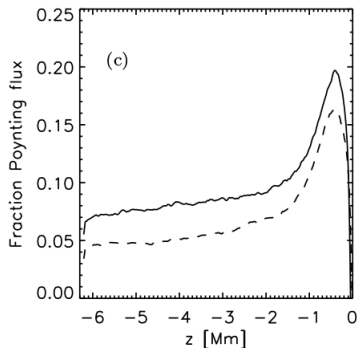

Figure 3: Fraction of energy transported by the Poynting flux relative to energy converted by the Lorentz force

- dashed line below solid line because saturation affects more $\vec{v} \cdot \left(\vec{j} \times \vec{B} \right)$ than $-(\vec{v} \times \vec{B}) \times \vec{B}$ (part of $\vec{P}$) ($\implies$ this fraction bigger because of saturation) and stronger saturation effect in solid line
- $\int_{z_{bottom}}^{z_{top}} E_{mag} dz$ 4 times bigger in solid line than dashed,
- but $\int_{z_{bottom}}^{z_{top}} \vec{v} \cdot \left(\vec{j} \times \vec{B} \right) dz$ comparable, 50% of the energy converted by pressure/buoyancy forces in the domain, 80% of the energy flux through the domain
- Most of the energy converted from kinetic to magnetic is preferentially dissipated in downflow regions, while work against the Lorentz force reduces the kinetic energy there. This changes the overall balance of the convective energy transport by reducing the contribution from the kinetic energy flux. We find in a non-magnetic convection simulation in 6 Mm depth a downward directed kinetic energy flux of about -0.3 F_{sun} , this value is reduced to 0.2 Fs in simulation O16bM

Dependence on domain size and resolution

- small scale **grid resolution dependence**
  Recently, Hotta et al. (2014) presented small-scale dynamo
  simulations in a global setup covering the convection zone up to 7
  Mm beneath the photosphere. Using a similar numerical approach,
  but a substantially lower grid spacing of 1100 km horizontally and
  375 km vertically, they were able to maintain a field with 0.15-0.25
  B_{eq} throughout the convection
  Overall field strength reached (their field near the top boundary
  falls short of our values by a factor of four, which is reflected in an
  energy conversion rate more than a factor of 10 lower)

- **small scale - large scale difference**
  Integrated over the entire convection zone, the energy conversion
  rate extracted from large-scale mean flows in mean field dynamo
  models (Rempel 2006), as well as three-dimensional global dynamo
  simulations (Nelson et al. 2013), is about two orders of magnitude
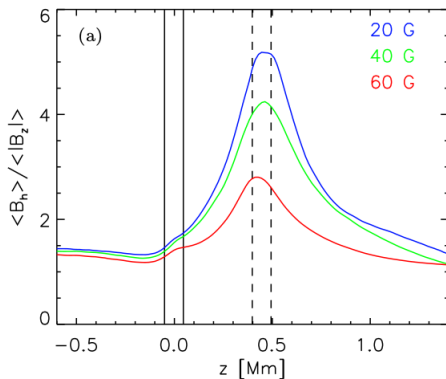 smaller.

Figure 4: Ratio of horizontal to vertical field strength as a function of height. Different colors refer to simulations with the average vertical field strength at $\tau = 1$ as indicated. The ratio of the horizontal to vertical field has a maximum at about 450 km above $\tau = 1$ and is strongly dependent on the overall field strength of the simulation and decreases with increasing field strength.
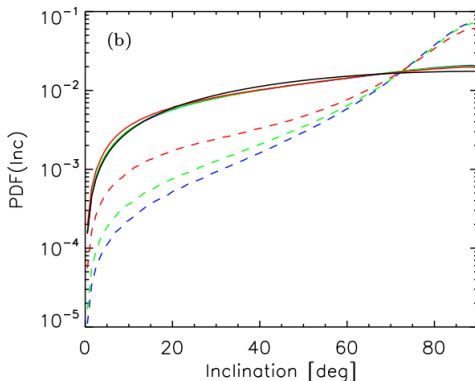
Figure 5: Probability distribution functions for the field inclination with respect to the vertical. Solid lines refer to the deep photosphere around $\tau = 1$, and dashed lines to about 450 km height. The black solid line indicates an isotropic distribution of field inclinations(agreement with solid lines).
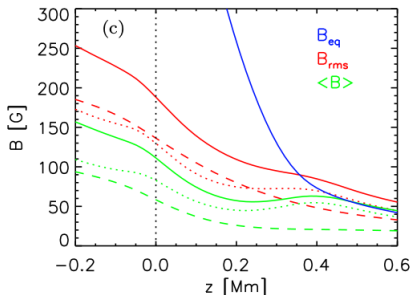
Figure 6: the magnetic field structure at the photosphere. Red (green) lines indicate the rms (mean) field strengths, while blue lines show the equipartition field strength. The meaning of the line styles: dashed (dotted) lines refer to the corresponding averages of vertical (horizontal) field components. Obs. peak at 450km above $\tau = 1$ also in the field strength

4.4 Distribution function: kG field concentrations
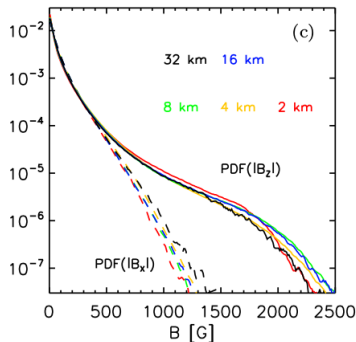
PDF robust ⟸ no dependence on resolution

Figure 7: Panel (c) shows the PDF for $|B_x|$ and $|B_z|$ at $\tau = 1$. We do not see a systematic dependence on resolution, differences for stronger field are mostly realization noise. For fields with less than 500 G strength the PDFs for $|B_x|$ and $|B_z|$ are essentially identical. Note that we show here the PDFs for the absolute values of the field components since the simulations do not have any net magnetic flux, leading to symmetric PDFs with respect to B = 0.

The shape of the PDF depends on field strength and domain size

- for $< |B_z| > 80$ G we find that 50% of the energy comes from fields with less than 500 G, kG field concentrations contribute about 16% to the total energy
- weaker field 60G energy from kG field concentrations drops to 9%
- 60G, larger domain it increases to 23%
- the filling factor of the kG field concentrations (area with field $< |B| >> 1$kG discussed in 3.4) is strongly field strength dependent. More than $< |B_z| > \approx 30$ - 40 G is required at $\tau = 1$ before they form and the filling factor increases steeply as the field strength increases beyond that threshold
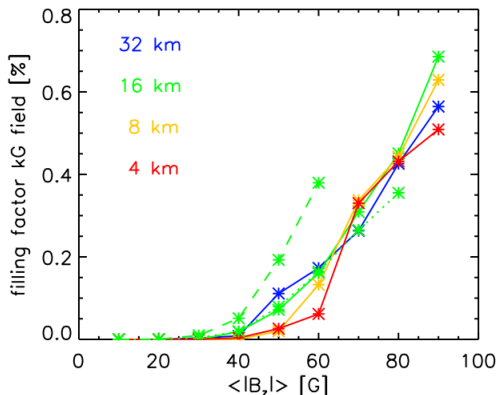
Figure 7. Filling factor of the kG field at $\tau = 1$. The solid lines are computed from simulations O32a–O4a, the dotted (dashed) lines correspond to O16b (O16bM). Field concentrations with more than 1 kG strength appear independent of resolution once $\langle|B_z|\rangle$ exceeds about 30–40 G. For 80 G the filling factor reaches about 0.45%. This fraction is not systematically dependent on resolution, but does increase with domain size (dashed line).

Comparing PDF for horizontal and vertical field

- Comparing the shape of normalized PDFs for vertical and horizontal field components, we find that the PDFs for the vertical field in the photosphere deviate substantially from those of horizontal field, as well as vertical field beneath the photosphere

- This is a strong hint for the presence of a convective intensification mechanism (Schussler 1990) that is restricted to the photosphere and mostly affects the vertical field
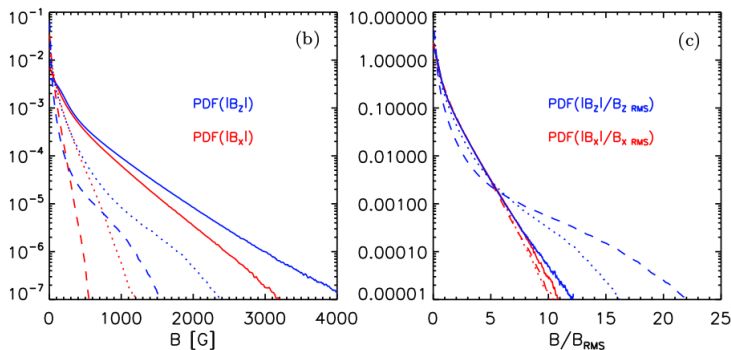
Figure 8: (b), (c) probability distribution functions for $|B_x|$ and $|B_z|$ for three different height levels in simulation O4a. Solid lines show quantities in 1 Mm depth, dotted lines on the $\tau = 1$, and dashed lines on the $\tau = 0.01$ levels. Panel (c) compares normalized PDFs, which allow for a direct comparison of the shape regardless of field strength

- not organized in the form of flux tubes, organized in sheets, often with alternating polarities. The kG flux concentrations are small knots along these sheets in which the field strength is increased temporarily due to dynamical effects
- it does not have a preferred scale around 100 km. We find the kG flux concentrations down to the smallest scales we can resolve
- The kG field present in our simulations does not produce a distinct feature in the PDFs like a secondary peak around kG field strength, which is found in many observations.
  These observation also indicate that the second peak is possibly caused by contributions from network field and may not be present for an inter-network field alone